

M. M. Bhatti\*, M. M. Rashidi, and I. Pop

# Entropy Generation with nonlinear heat and Mass transfer on MHD Boundary Layer over a Moving Surface using SLM

DOI 10.1515/nleng-2016-0021

Received May 17, 2016; accepted November 30, 2016.

**Abstract:** In this article, entropy generation with combined effects of thermal radiation and chemical reaction on MHD boundary layer over a moving surface has been investigated. The governing flow comprises of linear momentum equation, energy, and concentration equations which are modified with the help of similarity variables. The reduced resulting nonlinear coupled ordinary differential equations are solved with the help of Successive linearization method (SLM) and Chebyshev spectral collocation method. The impact of all the physical parameters is demonstrated numerically and graphically. A detailed analysis have been given for all the pertinent parameters such as Hartmann number, porosity parameter, Prandtl number, radiation parameter, suction/injection parameter, moving parameter, Brinkmann number, Reynolds number, chemical reaction parameter and Schmidt number on velocity, temperature, concentration and entropy profile as well as the Skin friction coefficient, Nusselt number and Sherwood number are also conducted. The numerical comparison has also been given to the existing published literature.

**Keywords:** Entropy; MHD; Heat and Mass Transfer; Chemical reaction; Thermal radiation

## 1 Introduction

During the past few years, thermal radiation plays an important role in the enhancement of heat transfer problems in which the convective heat transfer is not large. Furthermore, heat transfer with thermal radiation received a significant attention by various scientists due to its number of applications in aerodynamics [1]. The ratio of heat transfer on irregular and rough surfaces are very much higher as compared to smooth surfaces. Heat transfer between moving surfaces arises in a various industrial process such as hot extrusion of steel, lamination process, wind up roll, feed roll, conveyor belts melting and spinning process in the extrusion of polymers etc. Furthermore, moving surfaces involves in various applications like continuous casting process, fibre spinning, glass blowing etc. In all these applications, the study of heat transfer and flow field have a remarkable importance, since the performance of the products mainly relies upon the surface rate of heat transfer and skin friction coefficient. Some recent pertinent studies on moving surface can be found from the list of refs. [2–5].

Heat and mass transfer problems with chemical reaction have also numerous applications and involves in the various industrial processes such as drying, evaporation, oxygenation, geothermal reservoirs, hemodialysis, enhanced oil recovery, reverse osmosis, cooling of nuclear reactors and thermal energy storage. Moreover, the natural or mixed convection system which arises when a flow is analysed by inner volumetric forces and outer forcing system. Various practical diffusive activity includes the molecular diffusion of species in the existence of chemical reaction within the boundary or at the boundary. Hayat et al. [6] studied the effects of heat transfer and MHD over a permeable stretching surface with slip boundary conditions. Sheikholeslami et al. [7] investigated the combined effect of heat and mass transfer on MHD rotating viscous flow between a porous surface and a stretching sheet. Hayat et al. [8] analysed the influence of chemical reaction on unsteady three-dimensional non-Newtonian couple stress fluid over a stretching surface. Sheikholeslami

\*Corresponding Author: **M. M. Bhatti:** Shanghai Institute of Applied Mathematics and Mechanics, Shanghai University, Shanghai 200072, P. R. China, E-mail: muhammad09@shu.edu.cn; mubashirme@yahoo.com

**M. M. Rashidi:** Shanghai Key Lab of Vehicle Aerodynamics and Vehicle Thermal Management Systems, Tongji University, Shanghai 201804, China

**I. Pop:** Department of Mathematics, Babeş-Bolyai University, Cluj-Napoca, Romania

et al. [9] examined analytically the heat transfer effect on MHD rotating viscous fluid flow between stretching porous surface.

Different types of thermal systems are related to the mechanism of irreversibility which can be described with the help of entropy generation and are relevant to viscous dissipation, magnetic field, heat and mass transfer etc. To enhance this irreversibility process, various researchers used first law of thermodynamics but they found that the obtained results are unsatisfactory. Later, again various authors use the second law of thermodynamics to optimise these irreversibilities and observed that second law of thermodynamics is more efficient and reliable as compared to the first law of thermodynamics. Various authors investigated entropy generation in different media. For instance, Rashidi et al. [10] investigated entropy generation over a rotating porous disk with variable properties under the influence of MHD and slip. They analysed that disk source is the major point that helps in entropy generation. Kormurgoz et al. [11] studied entropy generation with the magnetic field in an inclined porous channel. He found that maximum entropy generation can be achieved in the absence of zero magnetic fields and zero porosity. Butt and Ali [12] examined the influence of irreversibility on unsteady, free convective hydromagnetic flow with thermal radiation past through a vertical porous plate. He found that entropy generation increases with the increment in thermal radiation and magnetic field while its behaviour is opposite due to porosity parameter. Rashidi et al. [13] investigated the entropy generation on MHD nanofluid over a rotating porous disk. Mahmud and Fraser [14] examined the entropy generation in a porous cavity under the influence of magnetohydrodynamics. He concluded that with the increment in the magnetic field, entropy generation increases. Tasnim et al. [15] examined analytically the influence of entropy generation in a porous medium under the effect of hydromagnetic. He concluded that maximum entropy generation is achieved near the walls of the channel. Some more pertinent studies on the said topic can be found from the list of refs. [16–19] and several therein.

On the other hand, Initially Magnetohydrodynamics was applied to geophysical and astrophysical problems. However, during the past few years, it has attracted towards a number of young researchers due to its applications in engineering and petroleum industry. Various devices have been invented that follow the principle of MHD such as MHD sensor, MHD generators, and MHD pumps. Magnetohydrodynamics sensors are very much helpful to measure the angular velocity in a navigation system of Aerospace engineering. The accuracy enhances with the size of Magnetohydrodynamics sensor. In various engi-

neering problems, Magnetohydrodynamics is applicable in liquid metal cooling of nuclear reactors, plasma confinement, and electromagnetic casting etc. In various microfluidics problems such as in microchannel design, Magnetohydrodynamics is considered as a fluid pump for creating a non-pulsating and continues the flow. Watanabe and Pop [20] investigated the Hall Effect on MHD boundary layer flow over a continuous moving flat plate. Abel et al. [21] studied the influence of thermal radiation and buoyancy force on Magnetohydrodynamics boundary layer viscoelastic fluid over a continuously moving stretching surface. Later, Salleh et al. [22] examined the heat transfer with Newtonian heating on boundary layer flow over a stretching sheet. Bhattacharyya et al. [23] investigated the impact of heat transfer with thermal radiation on micropolar fluid over a shrinking sheet through a porous medium. Some more pertinent studies can be seen from the refs. [24–29].

Motivation from the above studies, the aim of the present study is to analyse the entropy generation with combined effect of nonlinear thermal radiation and chemical reaction on MHD boundary layer flow over a moving surface. The governing equations for MHD boundary layer flow are formulated with the help of momentum, energy and concentration equations, which are further transformed into ordinary differential equations using similarity variables. Numerical solutions have been obtained with the help of Successive linearization method and Chebyshev spectral collocation method. The physical features of all the parameters are plotted and discussed. This paper is designed as follows; after the introduction in Sec. 1, Sec. 2 describes the mathematical formulation of the problem, Sec. 3 scrutinise the solution methodology, Sec. 4 illustrates the entropy generation analysis and finally, Sec. 5 is devoted to numerical results and discussion.

## 2 Mathematical formulation

Let us consider the steady 2-D irrotational flow of viscous, incompressible and electrically conducting fluid towards a moving surface in the presence of uniform external applied magnetic field  $B_0$ . We have selected a Cartesian coordinate system, in such a way that the flow is moving along  $x$ -axis whereas  $y$ -axis is considered along normal to it. The flow being confined to  $y > 0$ , the governing equation of continuity, momentum and energy equation for the MHD viscous fluid flow can be written as

$$\frac{\partial \tilde{u}}{\partial x} + \frac{\partial \tilde{v}}{\partial y} = 0, \quad (1)$$

$$\rho \left( \tilde{u} \frac{\partial \tilde{u}}{\partial x} + \tilde{v} \frac{\partial \tilde{u}}{\partial y} \right) = \mu \frac{\partial^2 \tilde{u}}{\partial y^2} + \left( \sigma B_0^2 + \frac{\mu}{k} \right) (\tilde{u}_e - \tilde{u}) + \tilde{u}_e \frac{d\tilde{u}_e}{dx}, \quad (2)$$

$$\tilde{u} \frac{\partial \tilde{T}}{\partial x} + \tilde{v} \frac{\partial \tilde{T}}{\partial y} = \tilde{\alpha} \frac{\partial^2 \tilde{T}}{\partial y^2} - \frac{1}{\rho c_p} \frac{\partial q_r}{\partial y}, \quad (3)$$

$$\tilde{u} \frac{\partial \tilde{C}}{\partial x} + \tilde{v} \frac{\partial \tilde{C}}{\partial y} = \tilde{D} \frac{\partial^2 \tilde{C}}{\partial y^2} - \tilde{y} (\tilde{C} - \tilde{C}_\infty), \quad (4)$$

their respective boundary conditions are given by

$$\tilde{u} = \tilde{u}_w(x), \tilde{T} = \tilde{T}_w(x), \tilde{C} = \tilde{C}_w(x), y = 0, \quad (5)$$

$$\tilde{u} \rightarrow \tilde{u}_e(x), \tilde{T} \rightarrow \tilde{T}_\infty, \tilde{C} \rightarrow \tilde{C}_\infty, y \rightarrow \infty. \quad (6)$$

With the help of Rosseland approximation, the radiative heat flux can be defined as

$$q_r = -\frac{4\tilde{\sigma}}{3\tilde{k}} \frac{\partial \tilde{T}^4}{\partial y}. \quad (7)$$

With the help of Taylor series, we expand  $\tilde{T}^4$  about  $\tilde{T}_\infty$ , we have

$$\tilde{T}^4 = 4\tilde{T}\tilde{T}_\infty^3 - 3\tilde{T}_\infty^4. \quad (8)$$

We have

$$\frac{\partial q_r}{\partial y} = -\frac{16\tilde{\sigma}\tilde{T}_\infty^3}{3\tilde{k}} \frac{\partial \tilde{T}}{\partial y}. \quad (9)$$

The similarity variables are defined as follows

$$\zeta = y \sqrt{\frac{\tilde{u}_e}{\nu x}}, \Phi = \sqrt{\nu x \tilde{u}_e} g(\zeta), \quad \theta(\zeta) = \frac{\tilde{T} - \tilde{T}_\infty}{\tilde{T}_w - \tilde{T}_\infty}, \Phi(\zeta) = \frac{\tilde{C} - \tilde{C}_\infty}{\tilde{C}_w - \tilde{C}_\infty}. \quad (10)$$

The stream function satisfying equation of continuity are defined as  $\tilde{u} = \partial \Phi / \partial y$  and  $\tilde{v} = -\partial \Phi / \partial x$ . Using Eq. (10) in Eq. (2) to Eq. (9), we get in simplified form as

$$g''' + \frac{1}{2} g g'' + \Gamma (1 - g') = 0, \quad (11)$$

$$\left( \frac{1}{Pr} + N_r \right) \theta'' + g \theta' = 0, \quad (12)$$

$$\Phi'' + Sc (g \Phi' - y \Phi) = 0. \quad (13)$$

The corresponding boundary conditions takes the new form

$$g(0) = S, g'(0) = \alpha, \theta(0) = 1, \Phi(0) = 1, \quad (14)$$

$$g'(\infty) = 1, \theta(\infty) = 0, \Phi(\infty) = 0, \quad (15)$$

where

$$y = \frac{\tilde{y}}{\tilde{a}}, Sc = \frac{\nu}{\tilde{\alpha}}, N_r = \frac{16\tilde{T}_\infty^3 \tilde{\sigma}}{3\tilde{k}\mu c_p}, Pr = \frac{\mu}{\tilde{\alpha}}, \quad M^2 = \frac{\sigma B_0^2}{\rho \tilde{a}}, K = \frac{\nu}{\tilde{a} \tilde{k}}, \Gamma = M^2 + K, \alpha = \frac{b}{\tilde{a}}. \quad (16)$$

The expression for Skin friction coefficient, local Nusselt number and Sherwood number in dimensionless form can be defined as [9]

$$\text{Re}_x^{1/2} C_f = g''(0), \text{Sh}_x / \text{Re}_x^{1/2} = -(1 + N_r) \theta'(0), \quad \text{Sh}_x / \text{Re}_x^{1/2} = -\Phi'(0). \quad (17)$$

where  $\text{Re}_x$  is a local Reynolds number.

### 3 Numerical Method

We apply the Successive linerization method (SLM) [30] to Eq. (11) with their boundary conditions in Eq. (14), by setting

$$g(\zeta) = g_I(\zeta) + \sum_{N=0}^{I-1} g_N(\zeta), \quad (I = 1, 2, 3, \dots), \quad (18)$$

where  $g_I$  are unknown functions which are obtained by iteratively solving the linearised version of the governing equation and assuming that  $g_I$  ( $0 \leq N \leq I - 1$ ) are known from previous iterations. Our algorithm starts with an initial approximation  $g_0(\zeta)$  which satisfy the given boundary conditions in Eq. (14) according to SLM. The suitable initial guess for the governing flow problem is

$$g_0(\zeta) = \zeta + \frac{S \exp[\zeta] + \alpha \exp[\zeta] - \alpha - \exp[\zeta] + 1}{\exp[\zeta]}. \quad (19)$$

We write the equation in general form as

$$\mathbf{L}(g, g', g'', g''') + \mathbf{N}(g, g', g'', g''') = 0, \quad (20)$$

where

$$\mathbf{L}(g, g', g'', g''') = g''', \quad (21)$$

and

$$\mathbf{N}(g, g', g'', g''') = \frac{1}{2} g g'' + \Gamma (1 - g'), \quad (22)$$

where  $\mathbf{L}$  and  $\mathbf{N}$  are the linear and non-linear part of Eq. (11). By substituting Eq. (18) in Eq. (11) and taking the linear terms only, we get

$$g_I''' + A_{0,I-1} g_I'' + A_{1,I-1} g_I' + A_{2,I-1} g_I = \mathbf{r}_{I-1}, \quad (23)$$

the corresponding boundary conditions becomes

$$g_i(0) = 0, g_i'(0) = 0, g_i'(\infty) = 0. \quad (24)$$

We solve Eq. (23) numerically by a well known method namely Chebyshev spectral collocation method. For numerical implementation, the physical region  $[0, \infty)$  is

truncated to  $[0, \Gamma_1]$ , we can take  $\Gamma_1$  to be sufficient large. With the help of following transformations this region is further transformed in to  $[-1, 1]$ , we have

$$\Omega = 2\Gamma_1^{-1}\zeta - 1. \quad (25)$$

We define the following discretization between the interval  $[-1, 1]$  and now we can apply Gauss-lobatto collocation points to define the nodes between  $[-1, 1]$  by

$$\Omega_J = \cos\left(\frac{\pi J}{N}\right), \quad (J = 0, 1, \dots, N), \quad (26)$$

with  $(N+1)$  number of collocation points. Chebyshev spectral collocation method based on the concept of differentiation matrix  $\mathbf{D}$ . This differentiation matrix maps a vector of the function values  $\mathbf{G} = [g(\Omega_0), \dots, g(\Omega_N)]^T$ , the collocation points to a vector  $\mathbf{G}'$  is defined as

$$\mathbf{G}' = \sum_{k=0}^N \mathbf{D}_{kj} g(\Omega_k) = \mathbf{D}\mathbf{G}, \quad (27)$$

the derivative of  $\mathbf{p}$  order for the function  $g(\Omega)$  can be written as

$$g^{(p)}(\Omega) = \mathbf{D}^p \mathbf{G}. \quad (28)$$

The entries of matrix  $\mathbf{D}$  can be computed by the method proposed by Bhatti et al. [30]. Now, applying the spectral method, with derivative matrices on linearized equation Eq. (23) and Eq. (24), we get the following linearized matrix system

$$\mathbf{A}_{I-1} \mathbf{G}_I = \mathbf{R}_{I-1}, \quad (29)$$

the boundary conditions takes the following form

$$\begin{aligned} g_I(\Omega_N) &= 0, \\ \sum_{k=0}^N \mathbf{D}_{Nk} g_I(\Omega_k) &= 0, \\ \sum_{k=0}^N \mathbf{D}_{0k} g_I(\Omega_k) &= 0, \\ \sum_{k=0}^N \mathbf{D}_{0k}^2 g_I(\Omega_k) &= 0, \end{aligned} \quad (30)$$

where

$$\mathbf{A}_{I-1} = \mathbf{D}^3 + A_{0,I-1} \mathbf{D}^2 + A_{1,I-1} \mathbf{D} + A_{2,I-1}. \quad (31)$$

In the above equation  $A_{s,I-1}$  ( $s = 0, 1, \dots, 3$ ) are  $(N+1) \times (N+1)$  diagonal matrices with  $A_{s,I-1}(\Omega_J)$  on the main diagonal and

$$\mathbf{G}_I = g_I(\Omega_J), \mathbf{R}_I = \mathbf{r}_I(\Omega_J). \quad (J = 0, 1, \dots, N) \quad (32)$$

After employing Eq. (30) on the linear matrix system in Eq. (29), we obtained the solutions for  $g_I$  by iteratively solving the system in Eq. (30). We obtain the solution for  $g(\zeta)$  from solving Eq. (30) and now Eq. (12) and Eq. (13) are now linear therefore, we will apply Chebyshev Pseudospectral method directly, which gives

$$\mathbf{B}\mathbf{H} = \mathbf{S}, \quad (33)$$

with their corresponding boundary conditions boundary conditions

$$\theta(\Omega_N) = 1, \theta(\Omega_0) = 0, \quad (34)$$

$$\Phi(\Omega_N) = 1, \Phi(\Omega_0) = 0, \quad (35)$$

where  $\mathbf{H} = (\theta(\Omega_J), \Phi(\Omega_J))$ ,  $\mathbf{B}$  is the set of coupled linear differential equations,  $\mathbf{S}$  is a vector of zeros, and all vectors in Eq. (33) are converted to diagonal matrix. We imposed the boundary conditions Eq. (34) and Eq. (35) on the first and last rows of  $\mathbf{B}$  and  $\mathbf{S}$ , respectively.

## 4 Entropy Generation Analysis

The volumetric entropy generation of the Newtonian fluid can be written as [34–39]

$$\begin{aligned} S_{Gen}''' &= \frac{\kappa}{\tilde{T}_\infty^2} \left[ \left( \frac{\partial \tilde{T}}{\partial y} \right)^2 + \frac{16\tilde{T}^3 \tilde{\sigma}}{3\tilde{k}} \left( \frac{\partial \tilde{T}}{\partial y} \right)^2 \right] \\ &+ \frac{\mu}{\tilde{T}_\infty^2} \left[ 2 \left( \frac{\partial \tilde{u}}{\partial x} \right)^2 + 2 \left( \frac{\partial \tilde{v}}{\partial y} \right)^2 + \left( \frac{\partial \tilde{u}}{\partial y} + \frac{\partial \tilde{v}}{\partial x} \right)^2 \right] \\ &+ \frac{\sigma B_0^2}{\tilde{T}_\infty} \tilde{u}^2 + \frac{\nu}{\tilde{k}\tilde{T}_\infty} \tilde{u}^2 + \frac{RD}{\tilde{T}_\infty} \left( \frac{\partial \tilde{T}}{\partial y} \frac{\partial \tilde{C}}{\partial y} + \frac{\partial \tilde{T}}{\partial x} \frac{\partial \tilde{C}}{\partial x} \right). \end{aligned} \quad (36)$$

In the above equation, entropy generation reveals three factors such as, the first term depicts a conduction effect which is due to the thermal radiation and heat transfer across a finite difference temperature (HTI). The second term depicts the fluid friction Irreversibility (FFI) and the third term is due to Diffusive Irreversibility (DI). It is also worth mentioning here that entropy generation occurs due to the sum of crossed terms with both concentration and thermal gradients and also a term which includes concentration gradient only. The entropy generation describes the non-dimensional form of entropy generation which represents the ratio between the characteristics entropy generation rate and the actual entropy generation rate. Thus, the characteristics entropy generation can be written as [34]

$$S_0''' = \frac{\kappa(\Delta T)^2}{x^2 \tilde{T}_\infty^2}. \quad (37)$$

Using Eq. (36) and Eq. (37), the entropy generation in dimensionless form can be written as

$$N_G = \frac{S_{Gen}'''}{S_0'''} = \text{Re}(1 + N_r)\theta'^2(\zeta) + \frac{\text{Re}B_r}{\Omega}g''^2(\zeta) + \frac{\text{Re}B_r}{\Omega}\Gamma g'^2(\zeta) + \text{Re}\lambda\left(\frac{\Lambda}{\Omega}\right)^2\Phi'^2(\zeta) + \text{Re}\lambda\left(\frac{\Lambda}{\Omega}\right)\Phi'(\zeta)\theta'(\zeta), \quad (38)$$

where  $\text{Re}$ ,  $B_r$  are the Reynolds number and Brinkman number and  $\Omega$  is the dimensionless temperature difference. These number are given in the following form

$$\text{Re} = \frac{\tilde{u}_e x}{\nu}, B_r = \frac{\mu \tilde{u}_w^2}{\kappa \Delta T}, \Omega = \frac{\Delta T}{T_\infty}, \lambda = \frac{RD\tilde{C}_\infty}{\kappa}, \Lambda = \frac{\Delta C}{\tilde{C}_\infty}. \quad (39)$$

## 5 Results and Discussion

This section deals with the numerical results of all the physical parameters involved. For this purpose Fig. 1 to Fig. 13 are plotted for velocity profile, temperature profile, concentration profile and entropy profile against suction/injection parameter, magnetic parameter, porosity parameter, moving parameter, Prandtl number, radiation parameter, chemical reaction parameter, Schmidt number, Reynolds number and Brinkmann number. The numerical results are presented in Table 1 for skin friction coefficient, Nusselt number, and Sherwood number. The variation of Moving parameter with Hartmann number and porosity parameter are summarised in Table 2. In Table 2 our results are very much similar with the existing published literature [3, 31–33] in the absence of magnetic field and porosity parameter ( $\Gamma = 0$ ). Fig. 1 shows the combined effect of magnetic field and porosity parameter on velocity. From this figure, we can observe that for larger values ( $\Gamma$ ) the velocity of the fluid is higher in magnitude. It can be noticed from Fig. 2 that with the increment in the suction parameter, it tends to raise the velocity of the fluid. Fig. 3 shows that when the moving parameter increases then it leads to decelerate the velocity of the fluid. However, when the moving parameter increases towards positive values than the boundary layer thickness increases as shown in Fig. 4.

Fig. 5 to Fig. 7 are plotted for temperature profile against various values of Prandtl number ( $Pr$ ), radiation parameter ( $N_r$ ), and suction/injection parameter ( $S$ ). It can easily observe from Fig. 5 that Prandtl number tends to reduce the temperature profile. Here, we can analyze that

for higher values of Prandtl number, momentum diffusivity dominates over thermal diffusivity. It is clear from Fig. 6 that temperature profile rises for larger values of radiation parameter ( $N_r$ ). It can be easily examined from Fig. 7 that when the suction parameter ( $S$ ) increases then the temperature profile diminishes. Fig. 8 to Fig. 10 represents the concentration profile against chemical reaction parameter ( $\gamma$ ), Schmidt number ( $Sc$ ) and suction/injection parameter ( $S$ ). It can be visualize from Fig. 8 that due to the greater impact of chemical reaction parameter ( $\gamma$ ), concentration profile tends to decrease. However, concentration profile behaves in a similar way for Schmidt number ( $Sc$ ) and suction/injection parameter ( $S$ ) as shown in Fig. 9 and Fig. 10. Fig. 11 to Fig. 14 are sketched for entropy generation profile against Brinkmann number ( $B_r$ ), Reynolds number ( $\text{Re}$ ), Radiation parameter ( $N_r$ ), magnetic and porosity parameter ( $\Gamma$ ). It is found that by increasing Brinkmann number ( $B_r$ ), Reynolds number ( $\text{Re}$ ), Radiation parameter ( $N_r$ ), magnetic and porosity parameter ( $\Gamma$ ), entropy profile increases.

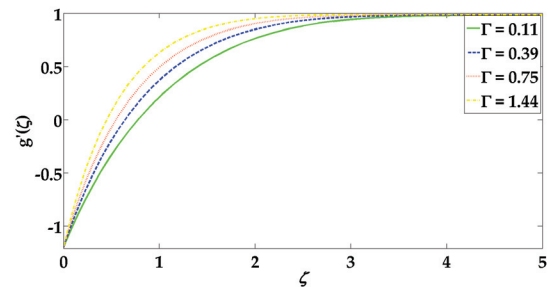


Fig. 1: Velocity profile for various values of ( $\Gamma$ ), when  $\alpha = -1.2$ ,  $S = 2$ ,  $Pr = 2$ ,  $N_r = 1$ ,  $\gamma = 0.5$ ,  $Sc = 1$ .

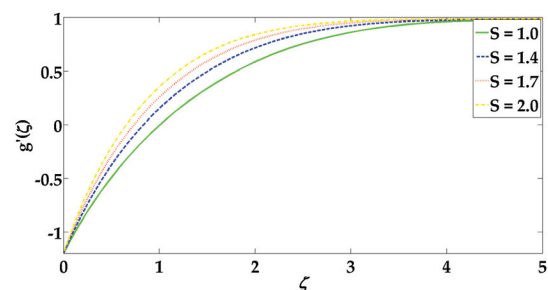


Fig. 2: Velocity profile for various values of Suction/injection parameter ( $S$ ), when  $\alpha = -1.2$ ,  $S = 2$ ,  $Pr = 2$ ,  $N_r = 1$ ,  $\gamma = 0.5$ ,  $Sc = 1$ .

Table 1: Numerical values of skin friction coefficients, local Nusselt number and Sherwood number.

$\Gamma$	$N_r$	$Pr$	$\alpha$	$S$	$Sc$	$y$	$C_f Re^{1/2}$	$Nu_x/Re^{1/2}$	$Sh_x/Re^{1/2}$
0.11	1.0	2.0	-1.2	2	1	0.5	2.2442	2.4033	2.0174
0.39							2.7214	2.4887	2.0525
0.75							3.1851	2.5558	2.0813
	0.9							2.5821	
	1.5							2.4923	
	2.0							2.4898	
		2.0						2.5558	
		3.0						2.8402	
		4.0						3.0121	
			-0.5				2.2869	2.8468	2.2431
			0.5				0.8123	3.1969	2.4429
			0.9				0.1662	3.3216	2.5151
				1.0			2.3890	1.2881	1.2046
				1.5			2.7712	1.9057	1.6258
				2.0			3.1851	2.5558	2.0813
					0.5				1.1711
					1.0				2.0813
					1.5				3.0058
						0.5			2.1225
						1.0			2.2766
						1.5			2.4498

Table 2: Variation of moving parameter ( $\alpha$ ) with Hartmann number and porosity parameter.

$\Gamma$	Klemp and Acrivos [31]	Hussaini et al. [32]	Ishak et al. [3]	Weidman et al. [33]	Present work
0					-0.3540
0.11	-0.3541	-0.3541	-0.3541	-0.3541	-0.3926
0.39					-0.4800
0.75					-0.5759
1.44					-0.7278

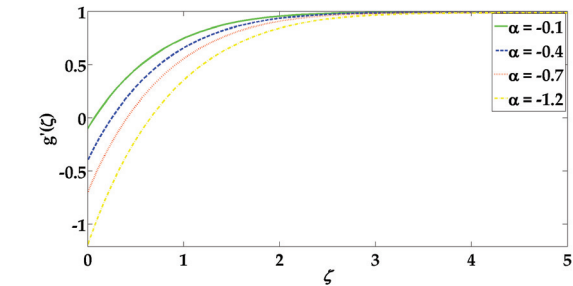


Fig. 3: Velocity profile for various values of  $\alpha(< 0)$ , when  $S = 2, Pr = 2, N_r = 1, y = 0.5, Sc = 1$

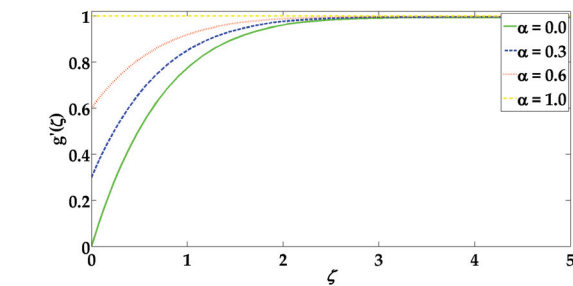
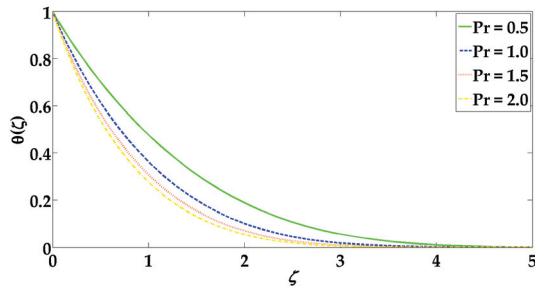
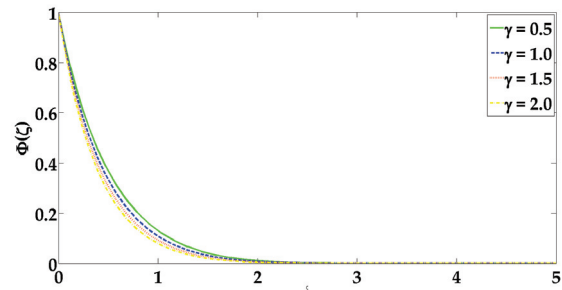


Fig. 4: Velocity profile for various values of  $\alpha(> 0)$ , when  $S = 2, Pr = 2, N_r = 1, y = 0.5, Sc = 1$





**Fig. 5:** Temperature profile for various values of Prandtl number ( $Pr$ ), when  $\alpha = -1.2$ ,  $S = 2$ ,  $N_r = 1$ ,  $\gamma = 0.5$ ,  $Sc = 1$ .



**Fig. 8:** Temperature profile for various values of ( $\gamma$ ), when  $\alpha = -1.2$ ,  $S = 2$ ,  $Pr = 2$ ,  $N_r = 1$ ,  $Sc = 1$ .

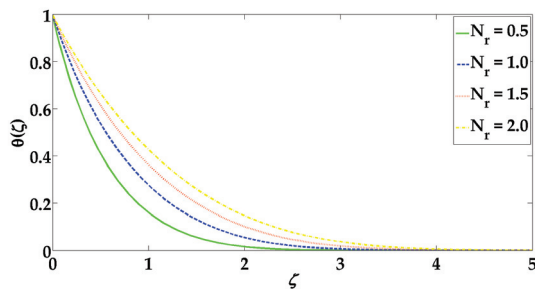


**Fig. 6:** Temperature profile for various values of Radiation parameter ( $N_r$ ), when  $\alpha = -1.2$ ,  $S = 2$ ,  $Pr = 2$ ,  $\gamma = 0.5$ ,  $Sc = 1$ .

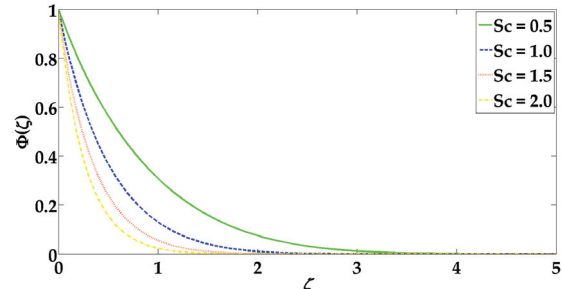


**Fig. 9:** Concentration profile for various values of ( $Sc$ ), when  $\alpha = -1.2$ ,  $S = 2$ ,  $Pr = 2$ ,  $N_r = 1$ ,  $\gamma = 0.5$ .

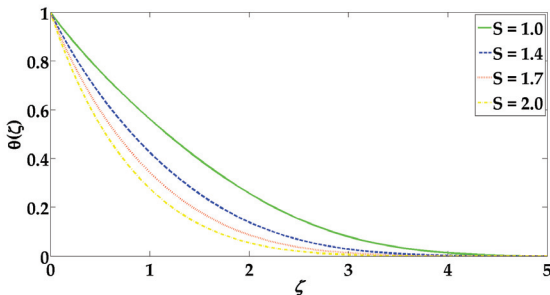


**Fig. 7:** Temperature profile for various values of suction/injection parameter ( $S$ ), when  $\alpha = -1.2$ ,  $Pr = 2$ ,  $N_r = 1$ ,  $\gamma = 0.5$ ,  $Sc = 1$ .

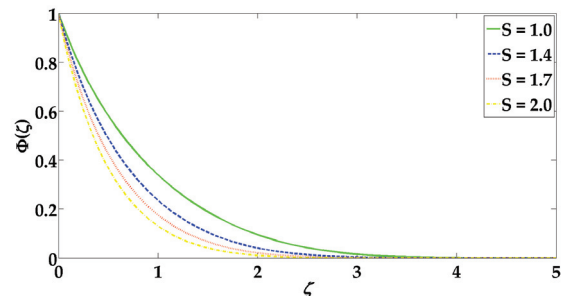


**Fig. 10:** Concentration profile for various values of ( $S$ ), when  $\alpha = -1.2$ ,  $S = 2$ ,  $Pr = 2$ ,  $N_r = 1$ ,  $\gamma = 0.5$ ,  $Sc = 1$ .

## 6 Conclusion

In this article, entropy generation with nonlinear thermal radiation and chemical reaction on MHD boundary layer flow has been examined numerically. Successive linearization method and Chebyshev spectral collocation method have been used to obtain the solution of the governing flow problem. The impact of all the parameters is plotted and discussed. The numerical comparison is also pre-

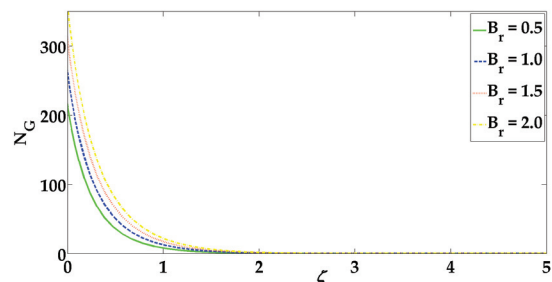


**Fig. 11:** Entropy profile for various values of ( $B_r$ ), when  $\alpha = -1.2$ ,  $S = 2$ ,  $Pr = 2$ ,  $N_r = 1$ ,  $\gamma = 0.5$ ,  $Sc = 1$ .

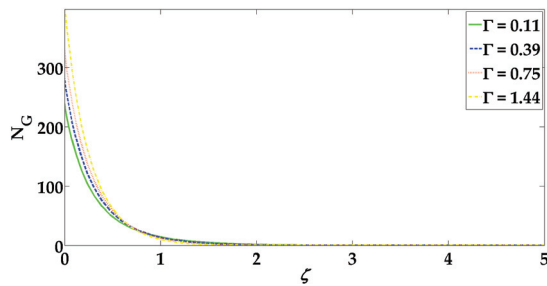


Fig. 12: Entropy profile for various values of ( $\Gamma$ ), when  $\alpha = -1.2$ ,  $S = 2$ ,  $Pr = 2$ ,  $N_r = 1$ ,  $\gamma = 0.5$ ,  $Sc = 1$ .

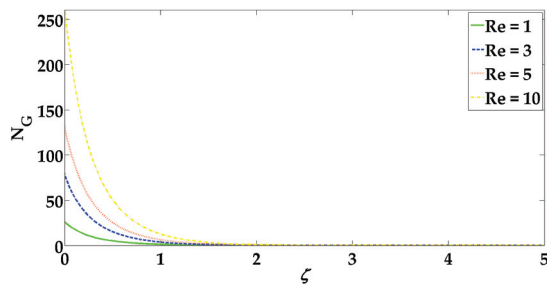


Fig. 13: Entropy profile for various values of ( $Re$ ), when  $\alpha = -1.2$ ,  $S = 2$ ,  $Pr = 2$ ,  $N_r = 1$ ,  $\gamma = 0.5$ ,  $Sc = 1$ .

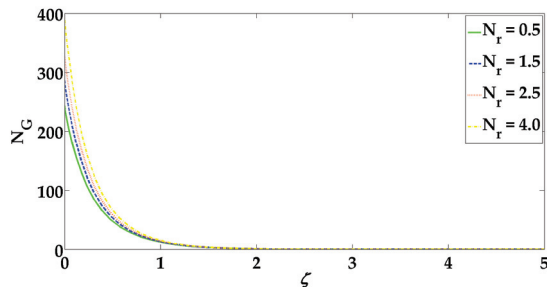


Fig. 14: Entropy profile for various values of ( $N_r$ ), when  $\alpha = -1.2$ ,  $S = 2$ ,  $Pr = 2$ ,  $\gamma = 0.5$ ,  $Sc = 1$ .

sented with the existing literature and found that present results are in good agreement. The main observations for the present flow problem are summarised below:

- Velocity of the fluid increases due to the impact of magnetic field and porosity.
- Temperature profile diminishes for large values of Prandtl number while it behaves opposite due to the effect of thermal radiation.
- Concentration profile decreases due to the increment in Schmidt number and chemical reaction parameter.
- Entropy profile behaves as an increasing function of all the pertinent parameters.

- Nusselt number and skin friction coefficient increase with a magnetic field and porosity parameter.
- Numerical comparison is also presented by taking  $\Gamma = 0$ , as a special case of our study.

## Nomenclature

$\tilde{u}, \tilde{v}$	Velocity components ( $m/s$ )
$x, y$	Cartesian coordinate ( $m$ )
$p$	Pressure ( $N/m^2$ )
$\tilde{k}$	Porosity parameter
$Re$	Reynolds number
$N_G$	Dimensionless entropy number
$t$	time ( $s$ )
$\bar{k}$	Mean absorption coefficient
$S$	Suction/injection parameter
$N_r$	Radiation parameter
$Pr$	Prandtl number
$M$	Hartmann number
$B_r$	Brinkman number
$B_0$	Magnetic field ( $Wb/m^2$ )
$S'''_{Gen}$	Local entropy generation ( $W/m^3 K$ )
$Sc$	Schmidt number
$\tilde{T}$	Temperature ( $K$ )
$a, b$	Constants
$c_p$	Specific heat at constant temperature ( $J/kgK$ )
$c_s$	Heat capacity
$\tilde{C}$	Concentration
$\tilde{D}$	Mass diffusion coefficient

## Greek Symbols

$\tilde{\alpha}$	Thermal conductivity of the fluid ( $W/mK$ )
$\alpha$	Moving parameter
$\nu$	Kinematic viscosity ( $kg/ms$ )
$\tilde{y}$	Reaction rate of solute
$\mu$	Viscosity of the fluid ( $kg/ms$ )
$\Phi$	stream function
$\rho$	Density of the fluid ( $kg/m^3$ )
$\kappa$	Thermal conductivity ( $W/mK$ )
$\Omega$	Dimensionless temperature difference
$\theta$	Dimensionless temperature
$\bar{\sigma}$	Steffan boltzman constant
$\sigma$	Electrical conductivity of the fluid ( $1/\Omega m$ )

## References

- [1] Ghosh SK, Beg OA (2008) Theoretical analysis of radiative effects on transient free convection heat transfer past a hot vertical surface in porous media. *Nonlinear Anal Model* 13:419–432



- [2] Bachok N, Ishak A, Pop I (2010) Boundary-layer flow of nanofluids over a moving surface in a flowing fluid. *Int J Therm Sci* 49:1663–1668
- [3] Ishak A, Nazar R, Bachok N, Pop I (2010) Melting heat transfer in steady laminar flow over a moving surface. *Heat mass transfer* 46 (2010) 463–468
- [4] Bhatti, M. M., Zeeshan, A., & Ellahi, R. (2016). Heat transfer analysis on peristaltically induced motion of particle-fluid suspension with variable viscosity: Clot blood model. *Computer Methods and Programs in Biomedicine*, 137, 115–124.
- [5] Bhatti, M. M., Zeeshan, A., Ijaz, N., Bég, O. A., & Kadir, A. (2016). Mathematical modelling of nonlinear thermal radiation effects on EMHD peristaltic pumping of viscoelastic dusty fluid through a porous medium duct. *Engineering Science and Technology, an International Journal*.
- [6] Hayat T, Qasim M, Mesloub S (2011) MHD flow and heat transfer over permeable stretching sheet with slip conditions. *Int J Numer Meth Fl* 66:963–975
- [7] Sheikholeslami M, Ashorynejad HR, Barari A, Soleimani S (2013) Investigation of heat and mass transfer of rotating MHD viscous flow between a stretching sheet and a porous surface. *Eng Comput* 30:357–378
- [8] Hayat T, Awais M, Safdar A, Hendi AA (2012) Unsteady three dimensional flow of couple stress fluid over a stretching surface with chemical reaction, *Nonlinear Anal Model* 17:47–59
- [9] Sheikholeslami M, Ashorynejad HR, Ganji DD, Kolahdooz A (2011) Investigation of rotating MHD viscous flow and heat transfer between stretching and porous surfaces using analytical method. *Math Prob Eng* 2011 Article ID 258734, 17 pages
- [10] Rashidi MM, Kavyani N, Abelman S (2014) Investigation of entropy generation in MHD and slip flow over a rotating porous disk with variable properties. *Int J Heat Mass Transfer* 70:892–917
- [11] Komurgoz G, Arikoglu A, Ozkol I (2012) Analysis of the magnetic effect on entropy generation in an inclined channel partially filled with porous medium, *Num Heat Transfer Part A* 61:786–99
- [12] Butt AS, Ali A (2013) Entropy effects in hydromagnetic free convection flow past a vertical plate embedded in a porous medium in the presence of thermal radiation. *Eur Phys J Plus* 128:51–65
- [13] Rashidi MM, Abelman S, Mehr NF (2013) Entropy generation in steady MHD flow due to a rotating porous disk in a nanofluid. *Int J Heat Mass Transfer* 62:515–525
- [14] Mahmud S, Fraser RA (2004) Magnetohydrodynamic free convection and entropy generation in a square porous cavity. *Int J Heat Mass Transfer* 47:3245–56
- [15] Tasnim SH, Shohel M, Mamun MAH (2002) Entropy generation in a porous channel with hydromagnetic effect. *Exergy, An International Journal* 2:300–8
- [16] Bhatti, M. M., Zeeshan, A., & Ellahi, R. (2016). Endoscope analysis on peristaltic blood flow of Sisko fluid with Titanium magneto-nanoparticles. *Computers in Biology and Medicine*, 78, 29–41.
- [17] Seth, G. S., Sharma, R., & Kumbhakar, B. (2016). Heat and mass transfer effects on unsteady MHD natural convection flow of a chemically reactive and radiating fluid through a porous medium past a moving vertical plate with arbitrary ramped temperature. *J. Appl. Fluid Mech*, 9(1), 103–117
- [18] Seth, G. S., & Sarkar, S. (2015). Hydromagnetic natural convection flow with induced magnetic field and nth order chemical reaction of a heat absorbing fluid past an impulsively moving vertical plate with ramped temperature. *BULGARIAN CHEMICAL COMMUNICATIONS*, 47(1), 66–79
- [19] Bhatti, M. M., Abbas, T., & Rashidi, M. M. (2016). Effects of thermal radiation and electromagnetohydrodynamic on viscous nanofluid through a riga plate. *Multidiscipline Modeling in Materials and Structures*, 12(4).
- [20] Watanabe T, Pop I (1995) Hall effects on magnetohydrodynamic boundary layer flow over a continuous moving flat plate. *Acta Mech* 108:35–47
- [21] Abel S, Prasad KV, Mahaboob A (2005) Buoyancy force and thermal radiation effects in MHD boundary layer visco-elastic fluid flow over continuously moving stretching surface. *Int J Therm Sci* 44:465–476
- [22] Salleh MZ, Nazar R, Pop I (2010) Boundary layer flow and heat transfer over a stretching sheet with Newtonian heating. *J Taiwan Inst Chem E* 41:651–655
- [23] Bhattacharyya K, Mukhopadhyay S, Layek GC, Pop I (2012) Effects of thermal radiation on micropolar fluid flow and heat transfer over a porous shrinking sheet. *Int J Heat Mass Trans* 55:2945–2952
- [24] Bhatti, M. M., Abbas, T., & Rashidi, M. M. (2016). Numerical Study of Entropy Generation with Nonlinear Thermal Radiation on Magnetohydrodynamics non-Newtonian Nanofluid Through a Porous Shrinking Sheet. *JOURNAL OF MAGNETICS*, 21(3), 468–475.
- [25] Seth, G. S., Sarkar, S., & Hussain, S. M. (2014). Effects of Hall current, radiation and rotation on natural convection heat and mass transfer flow past a moving vertical plate. *Ain Shams Engineering Journal*, 5(2), 489–503
- [26] Bhatti, M. M., Abbas, T., & Rashidi, M. M. (2016). A New Numerical Simulation of MHD Stagnation-Point Flow Over a Permeable Stretching/Shrinking Sheet in Porous Media with Heat Transfer. *Iranian Journal of Science and Technology, Transactions A: Science*, 1–7.
- [27] Bhatti, M. M., Abbas, T., Rashidi, M. M., Ali, M. E. S., & Yang, Z. (2016). Entropy Generation on MHD Eyring–Powell Nanofluid through a Permeable Stretching Surface. *Entropy*, 18(6), 224.
- [28] Bhatti, M. M., Abbas, T., Rashidi, M. M., & Ali, M. E. S. (2016). Numerical Simulation of Entropy Generation with Thermal Radiation on MHD Carreau Nanofluid towards a Shrinking Sheet. *Entropy*, 18(6), 200.
- [29] Bhatti, M. M., & Rashidi, M. M. (2016). Effects of thermodiffusion and thermal radiation on Williamson nanofluid over a porous shrinking/stretching sheet. *Journal of Molecular Liquids*.
- [30] Bhatti MM, Shahid A, Rashidi MM (2016) Numerical simulation of Fluid flow over a shrinking porous sheet by Successive linearization method. *Alexandria Eng J* 55:51–56
- [31] Klemp JB, Acrivos A (1972) A method for integrating the boundary-layer equations through a region of reverse flow. *J Fluid Mech* 53:177–191
- [32] Hussaini MY, Lakin WD, Nachman A (1987) On similarity solutions of a boundary layer problem with an upstream moving wall. *SIAM J Appl Math* 47:699–709
- [33] Weidman PD, Kubitschek DG, Davis AMJ (2006) The effect of transpiration on self-similar boundary layer flow over moving surfaces. *Int J Eng Sci* 44:730–737

- [34] Qing J, Bhatti MM, Abbas MA, Rashidi MM, Ali MES (2016) Entropy Generation on MHD Casson Nanofluid Flow over a Porous Stretching/Shrinking Surface. *Entropy* 18: 123
- [35] Bhatti, Muhammad Mubashir, Munawwar Ali Abbas, and Mohammad Mehdi Rashidi. Entropy generation for Peristaltic blood flow with Casson model and considering Magnetohydrodynamics effects. *Walailak Journal of Science and Technology (WJST)* 14.6 (2016).
- [36] Bhatti, M. M., Abbas, T., Rashidi, M. M. (2016). Entropy Generation as a Practical Tool of Optimisation for non-Newtonian Nanofluid Flow through a Permeable Stretching Surface using SLM. *Journal of Computational Design and Engineering*.
- [37] Abbas, T., Ayub, M., Bhatti, M. M., Rashidi, M. M., Ali, M. E. S. (2016). Entropy Generation on Nanofluid Flow through a Horizontal Riga Plate. *Entropy*, 18(6), 223.
- [38] Bhatti, M. M., Rashidi, M. M. (2016). Entropy Generation with Nonlinear Thermal Radiation in MHD Boundary Layer Flow Over a Permeable Shrinking/Stretching Sheet: Numerical Solution. *Journal of Nanofluids*, 5(4), 543–548.
- [39] Bhatti, M. M., Rashidi, M. M. (2016). Numerical simulation of entropy generation on MHD nanofluid towards a stagnation point flow over a stretching surface. *International Journal of Applied and Computational Mathematics*, 1–15.